Annals of Nuclear Energy 80 (2015) 151–165

Contents lists available at ScienceDirect

Annals of Nuclear Energy

journal homepage: www.elsevier.com/locate/anucene

A Multi-State Physics Modeling approach for the reliability assessment of Nuclear Power Plants piping systems

Francesco Di Maio [a,*], Davide Colli [a], Enrico Zio [a,b], Liu Tao [c], Jiejuan Tong [c]

[a] Energy Department, Politecnico di Milano, Via Ponzio 34/3, 20133 Milano, Italy
[b] Chair on System Science and Energetic Challenge, Fondation EDF, Ecole Centrale, Paris, and Supelec, Paris, France
[c] Institute of Nuclear and New Energy Technology, Beijing 100084, China

ARTICLE INFO

Article history:
Received 28 October 2014
Accepted 6 February 2015
Available online 24 February 2015

Keywords:
Piping reliability
Multi-State Physics Modeling
Degradation process
Markov Chain Model
Monte Carlo
Time-dependant transition rates
Nuclear Power Plant

ABSTRACT

A Multi-State Physics Modeling (MSPM) approach is here proposed for degradation modeling and failure probability quantification of Nuclear Power Plants (NPPs) piping systems. This approach integrates multi-state modeling to describe the degradation process by transitions among discrete states (e.g., no damage, micro-crack, flaw, rupture, etc.), with physics modeling by (physic) equations to describe the continuous degradation process within the states. We propose a Monte Carlo (MC) simulation method for the evaluation of the time-dependent transition rates between the states of the MSPM. Accountancy is given for the uncertainty in the parameters and external factors influencing the degradation process. The proposed modeling approach is applied to a benchmark problem of a piping system of a Pressurized Water Reactor (PWR) undergoing thermal fatigue. The results are compared with those obtained by a continuous-time homogeneous Markov Chain Model.

1. Introduction

Piping systems are one of the most risk-sensitive structural elements of Nuclear Power Plants (NPPs). Then, the analysis of these systems for the quantification of their failure probability is of utmost importance (Gopika et al., 2003). Different approaches have been applied for the estimation of piping systems failure probabilities. The most straightforward approach is to obtain estimates of piping component failure rates by statistical estimation based on field data collected from piping systems service experience, e.g. by Maximum Likelihood Estimation (MLE) approaches (Gosselin and Fleming, 1997). Alternatively, Probabilistic Fracture Mechanics (PFM) models can be used to predict crack initiation and growth from existing flaws (Verma and Srividya, 2011). To apply PFM models, the quantity and quality of information needed to perform the necessary computations are not negligible and the model evaluation can be time consuming, and even in cases where PFM approaches are appropriate, it is highly desirable to be able to benchmark and validate the results with some field data (Simola et al., 2002). In fact, for example, one limitation of this approach is that historical data reflect the influence of previous piping systems inspection programs, and, if changes to these programs are proposed, such changes may render the previous failure rate estimates no longer relevant (Fleming, 2004). To overcome these problems, a Markov Chain Model (MCM) has been proposed in (Fleming and Smit, 2008), in which the interaction between damage mechanisms and inspection, detection and repair strategies are explicitly defined and treated. However, transition rates between the degradation states and the holding times in any of the states of the MCM are assumed to be constant and to follow exponential distributions, respectively. This assumption is no longer acceptable when compared with field data of service experience (or when considering a new design of components with different geometry, material properties, degradation mechanisms and thermal–hydraulic behaviors) (Chatterjee and Modarres, 2008).

This paper presents the development and application of a novel framework for evaluating piping system reliability, specifically considering the situation of a new design of, or an already employed, piping system for which field data are not available or difficult to collect. The underlying model is non-Markovian because the transition rates are time-dependent, and include the uncertainties due to lack of knowledge of physical phenomena and parameters related to and influencing the degradation process (Li et al., 2012; Unwin et al., 2011). The approach undertaken is based on a Multi-State Physics Model (MSPM) and Monte Carlo (MC) simulation, which (i) accounts for the uncertain parameters and external factors influencing the process of transitions between degradation states and (ii) relaxes the constraints of time-indepen-

* Corresponding author.
E-mail address: francesco.dimaio@polimi.it (F. Di Maio).

http://dx.doi.org/10.1016/j.anucene.2015.02.007
0306-4549/

dent transition rates of continuous-time homogeneous MCM. The MSPM is, conceptually, a MCM in which the degradation processes (and thus, the transition rates) are described by physic model equations. In this work, the evaluation of the time-dependent transition rates is based on the outcomes of the Monte Carlo (MC) simulations of the degradation processes, directly described by physical models; this allows determining the distributions of the holding times of the components in the different states, from which the transition rates are derived. The knowledge added by the physics modeling and the inclusion of the effects of the uncertain parameters and the external factors which influence the degradation process allow a more realistic description of the piping system behavior and a more accurate estimation of its reliability (which, in the numerical case study considered avoids underestimation with respect to MCM, and the risk of exposing the system to catastrophic consequences in case of piping rupture).

The paper organization is as follows. Section 2 presents the general definition of the Multi-State Physics Model (MSPM) approach, also in consideration of the MCM approach, and the estimation procedure for the transition rates. Section 3 presents the MSPM application to a Pressurized Water Reactor (PWR) piping system. Section 4 contains the conclusions of the work.

2. Multi-state modeling for piping systems degradation

2.1. The continuous-time homogeneous Markov Chain Model (MCM)

Under the framework of Multi-State modeling, when the dynamics of component degradation is described by a continuous-time homogeneous Markov Chain Model (MCM), the transitions among a finite number M of discrete states $\overline{T}$, $\overline{T} = \{T_0, T_1, \ldots, T_M\}$, are modeled by constant rates $\lambda_{i,j}$ of transition from state i to state j, from which the state probability vector $\overline{P}(t)$ can be derived at any time instant t, $\overline{P}(t) = \{p_0(t), p_1(t), \ldots, p_M(t)\}$ (Li et al., 2012).

A general MCM to describe the piping systems degradation mechanisms is illustrated in Fig. 1, where $\overline{T} = \{S, F, L, R\}$ are the binary states healthy S (i.e., no detectable damage), degraded F and L (i.e., detectable flaw, detectable leak) and rupture R, respectively. The transition rates between states $\overline{T}$ are denoted as $\lambda_{S,F}$, $\lambda_{S,L}$, $\lambda_{S,R}$, $\lambda_{F,L}$, $\lambda_{F,R}$, $\lambda_{L,R}$, μ and ω. Transitions among states $\overline{T}$ can occur due to damage mechanisms at the pipe base metal (e.g., flow accelerated corrosion), on welds or in the heat-affected zone near welds (e.g. thermal fatigue), wall thinning, crack propagation, severe loading (e.g., water hammer and overpressure), and their various combinations (Fleming, 2004; Bush et al., 1996).

Under the assumption that all the transition rates are constant, the MCM equations consist of a set of linear differential equations with constant coefficients and the state probability vector $\overline{P}(t) = p_S(t), p_F(t), p_L(t), p_R(t)$ at any time t is determined by solving Eq. (1) (analytically or numerically) (Fleming, 2004):

$$\begin{cases} \frac{dp_S(t)}{dt} = -(\lambda_{S,L} + \lambda_{S,R} + \lambda_{S,F})p_S(t) + \omega p_F(t) + \mu p_L(t) \\ \frac{dp_F(t)}{dt} = \lambda_{S,F} p_S(t) - (\lambda_{F,L} + \lambda_{F,R} + \omega)p_F(t) \\ \frac{dp_L(t)}{dt} = \lambda_{S,L} p_S(t) + \lambda_{F,L} p_F(t) - (\lambda_{L,R} + \mu)p_L(t) \\ \frac{dp_R(t)}{dt} = \lambda_{S,R} p_S(t) + \lambda_{F,R} p_F(t) + \lambda_{L,R} p_L(t) \end{cases} \quad (1)$$

2.2. The Multi-State Physics Model (MSPM)

In this work, the MSPM transition rates, $\lambda_{i,j}(\tau_{i,j}, \overline{\delta})$, are assumed to be functions of the influencing factors $\overline{\delta}$ (i.e., the physical parameters used to model the degradation transition phenomena) and of $\tau_{i,j}$ (i.e., the holding time of the system in state i, provided that the arrival state will be j). On this premise, the objective of the MSPM framework is to solve for the state probability vector $\overline{P}(t) = \{p_S(t, \overline{\delta}), p_F(t, \overline{\delta}), p_L(t, \overline{\delta}), p_R(t, \overline{\delta})\}$ where, differently from the homogeneous MCM of Section 2.1, the transitions among states are described by τ-and $\overline{\delta}$-dependent transition rates. To obtain the state probability vector $\overline{P}(t, \overline{\delta})$ at each time t, the differential equations of Eq. (2) below need to be jointly solved:

$$\begin{cases} \frac{dp_S(t,\overline{\delta})}{dt} = -(\lambda_{S,L}(\tau_{S,L}, \overline{\delta}) + \lambda_{S,R}(\tau_{S,R}, \overline{\delta}) + \lambda_{S,F}(\tau_{S,F}, \overline{\delta}))p_S(t, \overline{\delta}) \\ \qquad +\omega p_F(t, \overline{\delta}) + \mu p_L(t, \overline{\delta}) \\ \frac{dp_F(t,\overline{\delta})}{dt} = \lambda_{S,F}(\tau_{S,F}, \overline{\delta})p_S(t, \overline{\delta}) - (\lambda_{F,L}(\tau_{F,L}, \overline{\delta}) + \lambda_{F,R}(\tau_{F,R}, \overline{\delta}) \\ \qquad +\omega)p_F(t, \overline{\delta}) \\ \frac{dp_L(t,\overline{\delta})}{dt} = \lambda_{S,L}(\tau_{S,L}, \overline{\delta})p_S(t, \overline{\delta}) + \lambda_{F,L}(\tau_{F,L}, \overline{\delta})p_F(t, \overline{\delta}) - \lambda_{L,R}(\tau_{L,R}, \overline{\delta}) \\ \qquad +\mu)p_L(t, \overline{\delta}) \\ \frac{dp_R(t,\overline{\delta})}{dt} = \lambda_{S,R}(\tau_{S,R}, \overline{\delta})p_S(t, \overline{\delta}) + \lambda_{F,R}(\tau_{F,R}, \overline{\delta})p_F(t, \overline{\delta}) + \lambda_{L,R}(\tau_{L,R}, \overline{\delta}) \\ \qquad +\mu)p_L(t, \overline{\delta}) \end{cases} \quad (2)$$

Notice that the four considered states $\overline{T}$ are mutually exclusive and form a complete set: thus, $p_S(t, \overline{\delta}) + p_F(t, \overline{\delta}) + p_L(t, \overline{\delta}) + p_R(t, \overline{\delta}) = 1$ at any time $t = 1, 2, \ldots, T_{miss}$, where T_{miss} is the mission time of the piping system. The calculation of the analytical solution $\overline{P}(t, \overline{\delta})$ of Eq. (2) with τ- and $\overline{\delta}$-dependent transition rates is a difficult (or even impossible in certain cases) task (Li et al., 2012; Lisnianski et al., 2008). To overcome this problem, a MC simulation framework is here proposed.

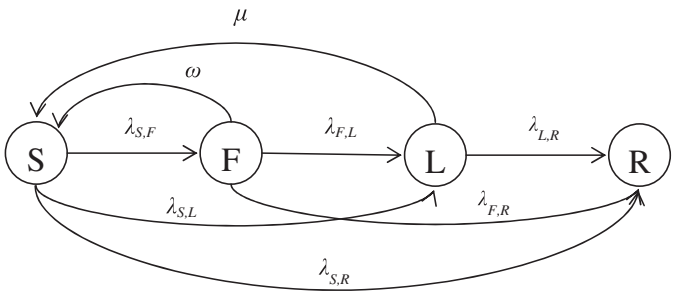

State
S - healthy, no detectable damage
F - detectable flaw
L - detectable leak
R - rupture

Transition Rates
$\lambda_{S,F}$ - flaw rate
$\lambda_{S,L}$ - leak failure rate given success
$\lambda_{F,L}$ - leak failure rate given a flaw
μ - repair rate via leak detection
$\lambda_{S,R}$ - rupture failure rate given success
$\lambda_{F,R}$ - rupture failure rate given flaw
$\lambda_{L,R}$ - rupture failure rate given a leak
ω - repair via In-Service Inspection (ISI) examinations

Fig. 1. Four-state MCM for degradation mechanisms in piping systems (Fleming, 2004).

2.2.1. Monte Carlo estimation of τ- and $\bar{\delta}$-dependent transition rates

The differential equations in Eq. (2) can be written in a general form as

$$\frac{d}{dt}p_i(t|\bar{\delta}) = \sum_{\substack{k=0 \\ k\neq i}}^{M} p_k(t|\bar{\delta})q_{k,i}(t|\bar{\delta})\lambda_k(t,\bar{\delta}) - p_i(t|\bar{\delta})\lambda_i(t,\bar{\delta}) \tag{3}$$

where $i = 1,2,\ldots,M$, $\lambda_i(t,\bar{\delta})$ is the total transition rate of departure from state i and

$$q_{k,i}(t|\bar{\delta}) = \frac{\lambda_{i,j}(t,\bar{\delta})}{\lambda_i(t,\bar{\delta})} \tag{4}$$

is the conditional probability that, given the transition out of any other state k, the arrival state will be i. The quantification of $\overline{P}(t,\bar{\delta})$ calls for the solution of Eq. (3), that can be obtained introducing the integrating factor $M_i(t,\bar{\delta}) = \exp\left[\int_0^t \lambda_i(t',\bar{\delta})dt'\right]$ (Li et al., 2012):

$$p_i(t|\bar{\delta}) = p_i(0)\cdot\exp\left[-\int_0^t \lambda_i(t',\bar{\delta})dt'\right] + \int_0^t \exp\left[-\int_{t'}^t \lambda_i(t'',\bar{\delta})dt''\right] \times \sum_{\substack{k=0 \\ k\neq i}}^{M} p_k(t'|\bar{\delta})q_{k,i}(t'|\bar{\delta})\lambda_k(t',\bar{\delta})dt' \tag{5}$$

Realistically, $\lambda_i(t|\bar{\delta})$, $i = 1,\ldots,M$, is unknown and, thus, cannot be used directly for calculating $p_i(t|\bar{\delta})$. Instead, based on the physical knowledge of the degradation mechanisms that determine the transitions among the states, the holding times τ_i can be estimated (by simulating the degradation mechanisms N_c times) and, then, the transition rate from state i to another state j can be indirectly determined. In this setting, the transition rates can be expressed as functions of $\tau_{i,j}$ as:

$$\lambda_{i,j}(\tau_{i,j},\bar{\delta}) = \frac{f(\tau_{i,j}|\bar{\delta})}{R(\tau_{i,j}|\bar{\delta})} \cong \lim_{\Delta\tau\to 0}\frac{F(\tau_{i,j}+\Delta\tau|\bar{\delta}) - F(\tau_{i,j}|\bar{\delta})}{(1-F(\tau_{i,j}|\bar{\delta}))\times(\Delta\tau)} \tag{6}$$

where $\tau_{i,j}$ is the holding time in state i, provided that the arrival state will be j, $R(\tau_{i,j}|\bar{\delta})$ is the reliability of the component at time $\tau_{i,j}$, $f(\tau_{i,j}|\bar{\delta})$ and $F(\tau_{i,j}|\bar{\delta})$ are the probability density function and cumulative distribution function of the holding time between states i and j, respectively.

The total transition rate λ_i of leaving state i towards any arrival state j, $j = 1,\ldots,M$, $j \neq i$ at time τ_i is, therefore, equal to:

$$\lambda_i(\tau_i,\bar{\delta}) = \sum_{\substack{j=0 \\ j\neq i}}^{M} \lambda_{i,j}(\tau_i,\bar{\delta}) \tag{7}$$

The total transition rate $\lambda_i(\tau_i,\bar{\delta})$, can, thus, be expressed as the convolution of all the transition rates that have determined any possible transition before time t, each with its holding time τ:

$$\lambda_i(t,\bar{\delta}) = \begin{cases} \int_0^t \lambda_1(t_1=\tau_1,\bar{\delta})dt_1 & \text{for } i=1 \\ \int_0^t \lambda_1(t_2=\tau_1,\bar{\delta})\lambda_2(t-t_2=\tau_2,\bar{\delta})dt_2 & \text{for } i=2 \\ \int_0^t\int_0^{t_n}\cdots\int_0^{t_3}\lambda_1(t_2=\tau_1,\bar{\delta}) & \\ \lambda_2(t_3-t_2=\tau_2,\bar{\delta})\ldots & \\ \lambda_{n-1}(t_n-t_{n-1}=\tau_{n-1},\bar{\delta}) & \\ \lambda_n(t-t_n=\tau_n,\bar{\delta})dt_2dt_3\ldots dt_n & \text{for } i=n \end{cases} \tag{8}$$

The lifetime t at which the system will be in state j^* is, therefore, equal to $t = \sum_{k=0}^{i}\tau_k$.

In the end, the procedure for calculating $\lambda_i(t,\bar{\delta})$ reduces to solving Eq. (6) that entails evaluating the cumulative distribution function $F(\tau_{i,j}|\bar{\delta})$ and the transition rates $\lambda_{i,j}(\tau_{i,j},\bar{\delta})$ as follows:

(1) *Build the physical models that describe the degradation process* (e.g., fatigue, thermal fatigue and stress corrosion cracking (SCC)).

(2) *Select a characteristic variable x (e.g. crack depth, crack length, etc.), that represents the degradation process state and its threshold value X_{cr}, that defines the transition from one state to another: the time $\tau_{i,j}$ at which the system moves from state i to state j is that at which $x = X_{cr}$.*

(3) *Sample the values of the parameters $\bar{\delta}$ of the physical models, treated as random variables whose values follow given distributions representing their uncertainties.*

(4) *Simulate the degradation process N_c times for estimating the state holding time $\tau_{i,j}$ distributions:* the algorithm for the estimation of the probability density function $f(\tau_{i,j}|\bar{\delta})$ and of the cumulative density function $F(\tau_{i,j}|\bar{\delta})$ is sketched in the following pseudo-code, where N_{succ} is the number of MC simulations in which $x \geqslant X_{cr}$, at time $\tau_{i,j}$ and N_c is the total number of trials. The time space is discretized by choosing a discrete timeline with $\Delta\tau$ as interval size.
Set the threshold dimension X_{cr}, the number of MC repeated trials N_c, the interval time size $\Delta\tau$ and the mission time T_{miss}.
Define N_{succ} as a vector of $T_{miss}/\Delta\tau$ elements, each one representing a discrete step on the timeline equal to $\Delta\tau$.
Consider a physics equation $x = g(\tau,\bar{\delta})$ that models x as a function of τ and $\bar{\delta}$.

For $N = 1 : N_c$
  $\tau = 0$
  Sample physics parameters $\bar{\delta}$ from their distributions
  $x = g(\tau,\bar{\delta})$
  While $x <= X_{cr}$
    $\tau = \tau + \Delta\tau$
    $x = g(\tau,\bar{\delta})$
  End While
  $Nsucc(\tau/\Delta\tau + 1) = Nsucc(\tau/\Delta\tau + 1) + 1$
End For
$f(\tau|\bar{\delta}) = N_{succ}/N_c$
$F(1) = f(1)$
For $N = 2 : T_{miss}/\Delta\tau$
  $F(N) = F(N-1) + f(N)$
End For

(5) *Estimate the transition rates by applying Eq. (6) with the selected $\Delta\tau$.*

2.2.2. Estimation of the state probability vector $\overline{P}(t,\bar{\delta})$

Once the transition rates $\lambda_{i,j}(\tau_{i,j},\bar{\delta})$ are estimated using Eq. (6), the state probability vector $\overline{P}(t,\bar{\delta})$ can be obtained by performing N_{max} direct MC simulations of the random walks through the states of the MCM. The time $\tau_{i,j}$ is sampled from $F(\tau_{i,j}|\bar{\delta})$ for each $j = 1,\ldots,M$; the holding time τ_i is $\tau_i = min(\tau_{i,j})$, whereas the arrival state j is the one that corresponds to $arg[min(\tau_{i,j})]$: the system enters state j at the respective time $\tau_{i,j}$. The state probability vector $\overline{P}(t,\bar{\delta})$ is, then, estimated by counting the number of visits $n(t)$ at time t to each state $i = 1,2,3,4$ (S, F, L, R, respectively) and dividing by the total number of random walk simulations N_{max} performed. The algorithm for the simulation of the process of component degradation on the time horizon $[0, T_{miss}]$ is sketched in the following pseudo-code.

Initialize the system at time $t_0 = 0$ and healthy state $i = 1(S)$. Set the total number of simulations N_{max}, the mission time T_{miss} and the state visit counters $n_i(t) = 0$, $i = 1,2,3,4$. Let τ_i be the time after which the system leaves state i.

While $N < N_{max}$
$i = 1$
$t = t_0$
While $t <= T_{miss}$
Sample the state holding times
$\tau_{i,j},\ j = 1,\ldots,M$, for $j \neq i$
The system moves to state j, at which corresponds the minimum $\tau_{i,j}$
$\tau_i = min(\tau_{i,j})$
$n_i(t:\tau_i) = n_i(t:\tau_i) + 1$
$t = t + \tau_i$
End While
$N = N + 1$
End While
$\overline{P}(t,\overline{\delta}) = \frac{1}{N_{max}}[n_1(t), n_2(t), n_3(t), n_4(t),]$

3. Application to a PWR piping system

3.1. System description

The modeling and simulation framework proposed is applied for the evaluation of the probability of rupture due to thermal fatigue of a mixing tee between the hot and cold legs during a Loss of Coolant Accident (LOCA) in the Reactor Cooling System (RCS) of a Pressurized Water Reactor (PWR) (Fleming, 2004; Radu et al., 2007a). The MCM model that describes this degradation process is sketched in Fig. 2. The simplification of the model with respect to Fig. 1 is based on the assumption that for fatigue damage mechanisms:

- Crack is initiated when the component shows a detectable Flaw (F).
- Crack propagates leading to a Leak (L) in case of circumferential crack that propagates to a through-wall circumferential crack and, then, to Rupture (R), or directly to Rupture (R) in case of fully-circumferential crack.
- The considered piping system is not subject to severe loading conditions: transitions between no damage state (S) to Rupture (R), or Leak (L) are not considered realistic.

The operating conditions of the downstream mixing tee are: pressure of 36 bar, hot leg water temperature at 180 °C and cold leg water temperature at 20 °C, pipe inner radius in the damage zone equal to $r_i = 120$ mm and outer radius to $r_o = 129$ mm (Radu et al., 2007b). The piping material is austenitic stainless steel 304L and the maximum temperature fluctuation ($\Delta\theta_{max}$), due to turbulent mixing or vortices on the inner surface of the pipe is estimated to be 120 °C (Radu et al., 2007b).

In what follows, we perform the reliability assessment of the piping system considering τ- and $\overline{\delta}$-dependent transition rates on a mission time $T_{miss} = 100$ years. T_{miss} has been chosen reasonably longer than a typical NPP lifetime of 40 years, to give account to possible life extension. We resort to the MSPM approach introduced in Section 2.2; the results will be compared with the MCM solutions obtained in Fleming (2004) for a typical PWR RCS piping system.

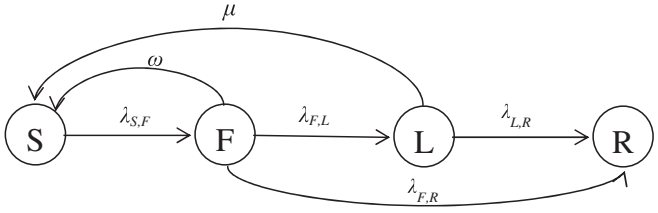

Fig. 2. MCM for a PWR component subjected to thermal fatigue (Fleming, 2004).

3.2. Monte Carlo estimation of τ- and $\overline{\delta}$-dependent transition rates

3.2.1. Transition rate $\lambda_{S,F}(\tau_{S,F}, \overline{\delta})$

The crack onset (i.e., the transition between states Safe (S) and Flaw (F)) on the tee piping component connecting the hot and cold legs of a RCS of a PWR, due to thermal fatigue, can be represented as in Fig. 3 and modeled referring to the total equivalent strain rate $x = \varepsilon_{eq}^{tot}$, that can be calculated as:

$$\varepsilon_{eq}^{tot} = K_\upsilon \cdot \varepsilon_{eq}^{elastic} \tag{9}$$

where K_υ and $\varepsilon_{eq}^{elastic}$ are functions of the effective equivalent stress intensity range $\Delta\sigma_{eq}$. Thus, (Ancelet et al., 2007):

$$\varepsilon_{eq}^{tot} = K_\upsilon(\Delta\sigma_{eq}) \cdot \frac{2\cdot(1+\upsilon)}{3}\frac{\Delta\sigma_{eq}}{E} \tag{10}$$

where υ is the Poisson coefficient, $K_\upsilon(\Delta\sigma_{eq})$ can be found by empirical correlation (plotted in Fig. 4), whereas $\Delta\sigma_{eq}$ is equal to (Radu et al., 2007b):

$$\Delta\sigma_{eq} = \sqrt{\frac{(\Delta\sigma_r - \Delta\sigma_\vartheta)^2 + (\Delta\sigma_z - \Delta\sigma_\vartheta)^2 + (\Delta\sigma_r - \Delta\sigma_z)^2}{2}} \tag{11}$$

where $\Delta\sigma_i,\ i = r,z,\vartheta$, are the maximum stress intensities ranges due to radial (σ_r), axial (σ_z) and hoop (σ_ϑ) thermal stresses, respectively. To evaluate the thermal stresses σ_r, σ_z and σ_ϑ, because of the simple geometry the pipe can be represented as a hollow cylinder and it is possible to use the analytical solutions proposed in Radu et al. (2007a), in which the piping system is assumed to be subjected to sinusoidal transients of thermal loads $\theta(\omega,\theta_0)$ that well approximate the cold and hot leg mixing phenomenon occurring at the tee piping component.

Therefore, the radial, hoop and axial stresses are (Radu et al., 2007a):

$$\sigma_r(r,\omega,\theta_0,k) = \frac{\alpha\cdot E}{1-\upsilon}\cdot\left[-\frac{1}{r^2}\cdot I_1(r,\omega,\theta_0,k) + \frac{r^2-r_i^2}{r^2\cdot(r_o^2-r_i^2)}\cdot I_2(r,\omega,\theta_0,k)\right] \tag{12}$$

$$\sigma_\vartheta(r,\omega,\theta_0,k) = \frac{\alpha\cdot E}{1-\upsilon}\cdot\left[\frac{1}{r^2}\cdot I_1(r,\omega,\theta_0,k) + \frac{r^2-r_i^2}{r^2\cdot(r_o^2-r_i^2)}\cdot I_2(r,\omega,\theta_0,k) - \theta(r,\omega,\theta_0,k)\right] \tag{13}$$

$$\sigma_z(r,\omega,\theta_0,k) = \frac{\alpha\cdot E}{1-\upsilon}\cdot\left(\frac{2\upsilon}{r_o^2-r_i^2}\cdot I_2(r,\omega,\theta_0,k) - \theta(r,\omega,\theta_0,k)\right) \tag{14}$$

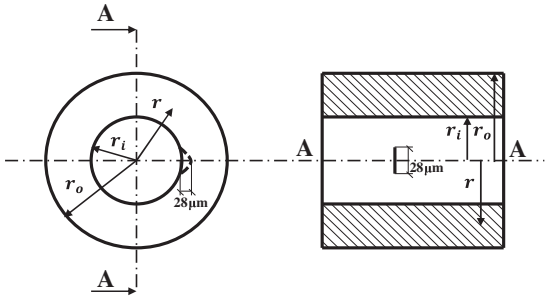

Fig. 3. Circumferential crack onset.

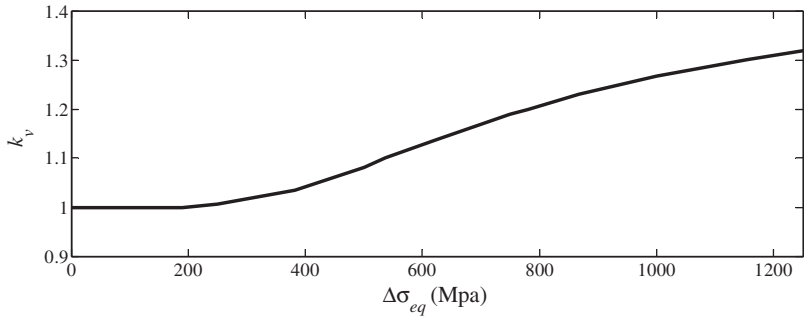

Fig. 4. Evolution of $k_v(\Delta\sigma_{eq})$.

Table 1
Parameters values and uncertainties.

Parameter	Description	Unit	Type of distribution	Lower value	Upper value
f	Frequency of temperature wave	Cycle/s	uniform	10^{-2}	100
Θ_0	Amplitude of temperature wave	°C	uniform	0	60
Parameter	Description	Unit	Value		
E	Modulus of elasticity	N/m^2	177×10^9		
α	Thermal expansion coefficient	1/°C	16.4×10^{-6}		
υ	Poisson coefficient	/	0.3		
k	Thermal diffusivity coefficient	m^2/s	3.93×10^{-6}		

where r is the radial distance from the center of the pipe, $\omega = 2\pi f$ and θ_0 are the frequency and amplitude of the temperature sinusoidal wave, respectively, k is the thermal diffusivity coefficient, α is the thermal expansion coefficient, E is the modulus of elasticity. The mathematical relationships for $I_1(r,\omega,\theta_0)$, $I_2(r,\omega,\theta_0)$ and the temperature distribution across the wall thickness $\theta(r,\omega,\theta_0)$ are given in Appendix A, with the theoretical details. Table 1 lists the parameters $\overline{\delta} = (f,\theta_0,E,\alpha,v,k)$, together with their distributions, affecting the model behavior and, thus, the crack onset.

For a given value of $x = \varepsilon_{eq}^{tot}$, the piping system experiences a circumferential crack onset (with initial crack depth and length equal to $x_1^{in} = x_2^{in} = 28$ μm (Varfolomeyev, 2006; Sester et al., 2000)), after a number of thermal cycles N_f that is given by the empirical correlation shown in Fig. 5, relating x to N_f (Ancelet et al., 2007). The state holding time $\tau_{S,F}$ for a specific set of values of $\overline{\delta}$ affecting the duration of the crack onset is, thus, calculated from N_f as:

$$\tau_{S,F}(years) = \frac{N_f}{f \cdot 3600 \cdot 24 \cdot 365} \tag{15}$$

where we consider 365 days per year, 24 h per day and 3600 s per hour. The probability distribution of $\tau_{S,F}$ is estimated by applying the MC simulation proposed at item (4) of Section 2.2.1, with a number of simulations $N_c = 10,000$. For each one of these N_c trials, ε_{eq}^{tot} is evaluated applying Eqs. (9)–(14) given a sampled batch of values of the parameters $\overline{\delta}$ (Table 1): N_c values of N_f are collected and the probability density function $f(\tau_{S,F}|\overline{\delta})$ and cumulative distribution function $F(\tau_{S,F}|\overline{\delta})$ can be built (shown in Figs. 6 and 7, respectively). By applying Eq. (6) with a time step of one year ($\Delta\tau = 1$), the transition rate $\lambda_{S,F}(\tau_{S,F},\overline{\delta})$ is computed (shown in Fig. 8).

The cumulative distribution function $F(\tau_{S,F}|\overline{\delta})$ describing the (uncertain) timing of the onset of the degradation process, reaches a value of 0.29 at $\tau_{S,F} = 100$ years: this confirms that (i) the mixing tee between the hot and cold legs is a resistant component capable of withstanding the onset of a flaw due to thermal fatigue for a very long period of time, and that (ii) even if unlikely during the life of an NPP, if a crack onset occurs, it appears in the early stage of the component life (as shown in Figs. 6 and 8).

3.2.2. Transition rate $\lambda_{F,L}(\tau_{F,L},\overline{\delta})$

The transition between states Flaw (F) (i.e., the onset of a circumferential crack on the inner pipe surface) and Leak (L) (i.e., a through-wall circumferential crack) is determined when the crack propagating in the radial direction, reaches the piping wall dimension $l = r_o - r_i$ (shown in Fig. 9). Thus, the critical value of the characteristic variable (i.e., the crack depth x_1) is $X_{cr,1} = l = 9$ mm.

We assume that the crack growth rate dx_1/dN follows a generalized Paris law Eq. (16) (Kozin and Bogdonoff, 1989; Di Maio and Zio, 2013):

$$\frac{dx_1}{dN} = C \cdot (\Delta K_{eff}(x_1))^n \tag{16}$$

where N is the number of thermal cycles, C and n are material coefficients (Zio and Di Maio, 2012) and ΔK_{eff} is the effective stress intensity factor range, that can be expressed as a function of the maximum stress intensity factor range ΔK_I and of a parameter $q(R)$ (Radu et al., 2007b):

$$\Delta K_{eff}(\sigma_z,x_1) = q(R) \cdot \Delta K_I(\sigma_z,x_1) \tag{17}$$

where σ_z is the axial stress of Eq. (14) and $\Delta K_I(\sigma_z,x_1)$ and $q(R)$ are defined as in Eqs. (18)–(21):

$$\Delta K_I(\sigma_z,x_1) = K_I^{max}(\sigma_z,x_1) - K_I^{min}(\sigma_z,x_1) \tag{18}$$

$$R(\sigma_z,x_1) = \frac{K_I^{min}(\sigma_z,x_1)}{K_I^{max}(\sigma_z,x_1)} \tag{19}$$

$$q(R) = \frac{1-0.5R}{1-R} \quad \text{if R} < 0 \tag{20}$$

$$q(R) = \frac{1}{1-0.5R} \quad \text{if R} > 0 \tag{21}$$

To calculate $K_I(\sigma_z,x_1)$, and its maximum ($K_I^{max}(\sigma_z,x_1)$) and minimum ($K_I^{min}(\sigma_z,x_1)$), we suppose that:

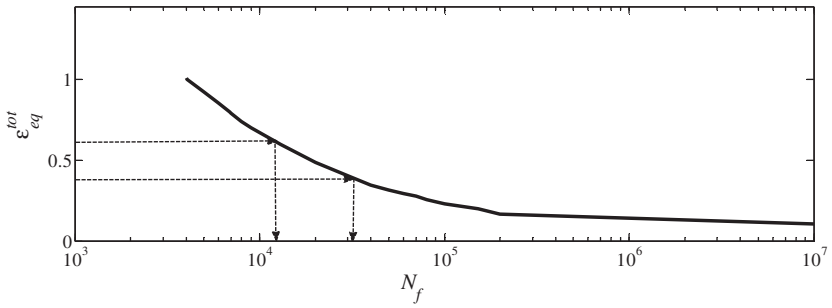

Fig. 5. Total equivalent strain rate ε_{eq}^{tot} vs number of cycles to failure $\boldsymbol{N_f}$ (Ancelet et al., 2007).

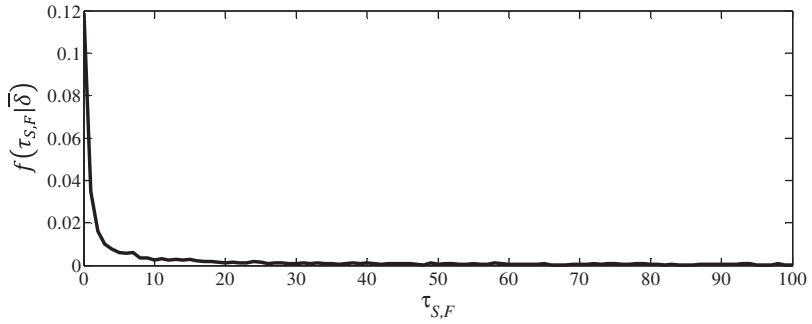

Fig. 6. Probability density function of the state holding time $\tau_{S,F}$.

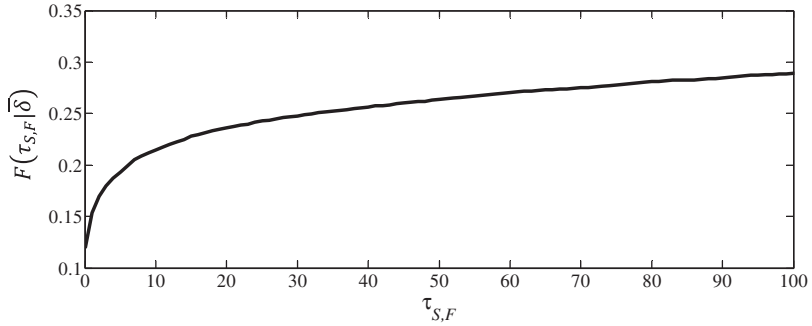

Fig. 7. Cumulative distribution function of the state holding time $\tau_{S,F}$.

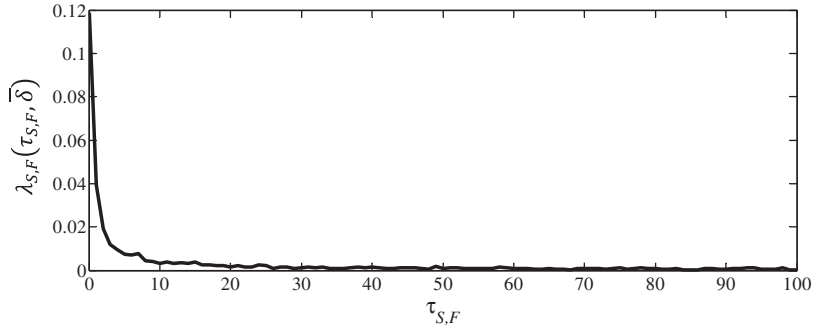

Fig. 8. Transition rate between states ***S*** and ***F***.

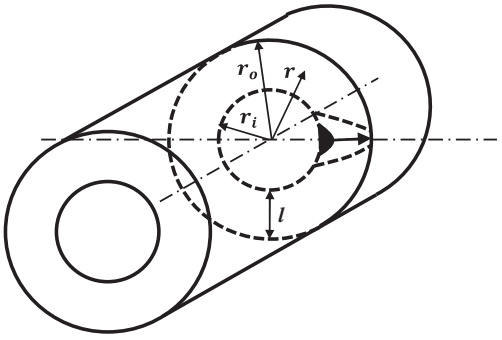

Fig. 9. Circumferential crack onset.

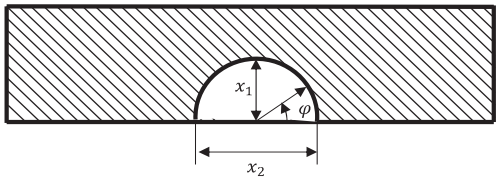

Fig. 10. Circumferential crack for a cylinder that approximates a flat plate.

Table 2
Paris law equation parameter values.

Parameter	Description	Unit	Value
n	Material coefficient		4
C	Material coefficient	m/cycle	7.5×10^{-13}

- the crack propagates radially such that the ratio between crack depth (x_1) and crack length (x_2) is equal to 1 (Ancelet et al., 2007) (i.e., when the crack depth reaches the wall thickness dimension, at the inner surface of the pipe, the crack length is equal to the wall thickness l)
- l/r_i is small enough to approximate the cylinder to a flat plate, in fact, for $l/r_i < 0.1$ the specific model for circumferential crack propagation in a hollow cylinder cannot be used, and the K_I solution is approximated using the flat plate model.
- the propagation phenomenon is studied at the deepest point of the crack ($\varphi = \pi/2$, see Fig. 10).

Theoretical details are given in Appendix B.

Tables 1 and 2 list the parameter $\bar{\delta} = (f, \theta_0, E, \alpha, v, k, n, C)$ and the distributions used in the evaluation of $\Delta K_{eff}(\sigma_z, x_1)$ and N (Chapuliot et al., 2005).

The number of cycles (N) needed to propagate a circumferential through-wall crack, starting from a circumferential crack onset, is given by:

$$N = \int_{x_1^{in}}^{X_{cr,1}} \frac{dx_1}{C \cdot (\Delta K_{eff}(\sigma_z, x_1))^n} \tag{22}$$

The equation has been solved using a MATLAB solver. The state holding time $\tau_{F,L}$ for a specific set of $\bar{\delta}$ affecting the radial propagation of the crack is, thus, calculated from N as:

$$\tau_{F,L}(years) = \frac{N}{f \cdot 3600 \cdot 24 \cdot 365} \tag{23}$$

The probability distribution of $\tau_{F,L}$ is estimated by applying the MC simulation proposed at item (4) of Section 2.2.1, with a number of trials $N_c = 10,000$. For each one of these N_c trials, $\Delta K_{eff}(\sigma_z, x_1)$ is evaluated given a sampled batch of values of the parameters $\bar{\delta}$ (Tables 1 and 2). Thus, the distributions $f(\tau_{F,L}|\bar{\delta})$ and $F(\tau_{F,L}|\bar{\delta})$ can be built (shown in Figs. 11 and 12, respectively). By applying Eq. (6) with a time step of one year ($\Delta\tau = 1$), the transition rate $\lambda_{F,L}(\tau_{F,L}, \bar{\delta})$ is computed (shown in Fig. 14).

The cumulative distribution function $F(\tau_{F,L}|\bar{\delta})$ of Fig. 12, describing the (uncertain) timing of the transition between states F and L, reaches a value of 0.10 at $\tau_{F,L} = 100$ years, showing that, (hopefully) the laps of time considered is not enough to guarantee that the crack onset propagates radially till a through-wall crack and generates a leakage phenomenon. The transition rate distribution $\lambda_{F,L}(\tau_{F,L}, \bar{\delta})$, shown in Fig. 13 and describing the variation of the probability of the system to leave states F to enter state L, shows a discontinuity from $\lambda_{F,L}(9, \bar{\delta}) = 0$ to $\lambda_{F,L}(10, \bar{\delta}) = 0.0016$ and a larger value of $\tau_{F,L}$ around $10 \leqslant \tau_{F,L} \leqslant 20$ years. This leads us to conclude that the circumferential crack that propagates across the piping wall needs at least 10 years to reach a through-wall circumferential characteristic. Moreover, Figs. 11 and 13 show that the estimation of $f(\tau_{F,L}|\bar{\delta})$ and $\lambda_{F,L}(\tau_{F,L}, \bar{\delta})$ provided by the crude MC simulation of Section 2.2.1 is more irregular than $f(\tau_{S,F}|\bar{\delta})$ and $\lambda_{S,F}(\tau_{S,F}, \bar{\delta})$ of Figs. 6 and 8. This can be improved by resorting to more efficient MC techniques able to dealing with low probability estimation (Zio and Pedroni, 2011).

3.2.3. Transition rate $\lambda_{F,R}(\tau_{F,R}, \bar{\delta})$

A piping system subjected to thermal fatigue may also break without showing any leakage phenomenon (i.e., the transition between states Flaw (F) and Rupture (R)), This event can be modeled considering two stages:

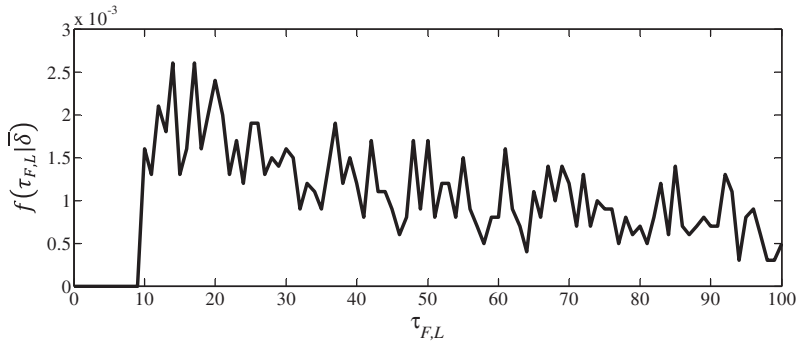

Fig. 11. Probability density function of the state holding time $\tau_{F,L}$.

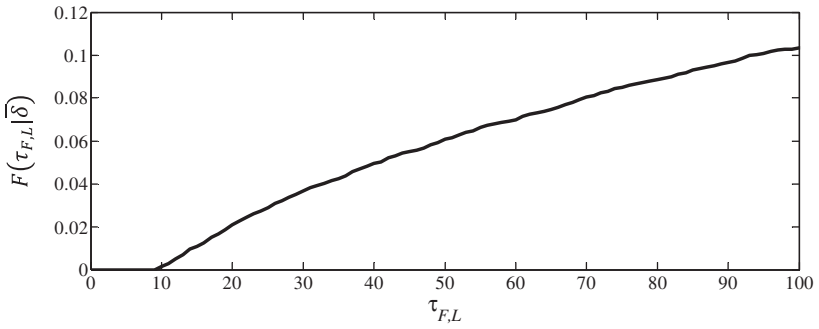

Fig. 12. Cumulative distribution function of the state holding time $\tau_{F,L}$.

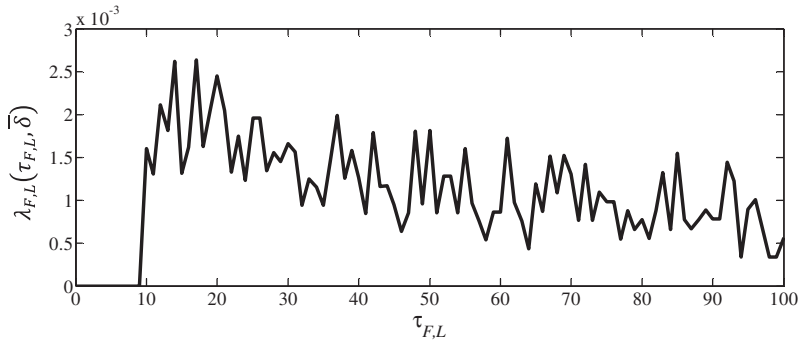

Fig. 13. Transition rate from states F to state L.

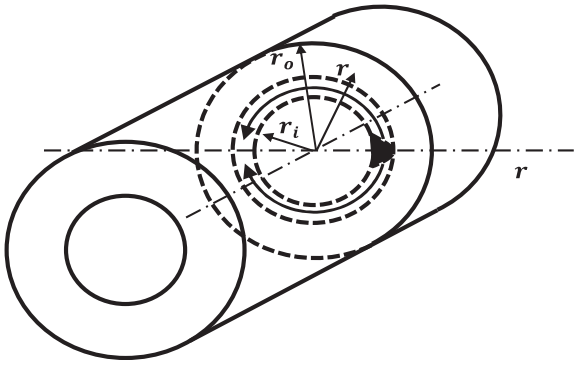

Fig. 14. Circumferential crack propagating along the circumference.

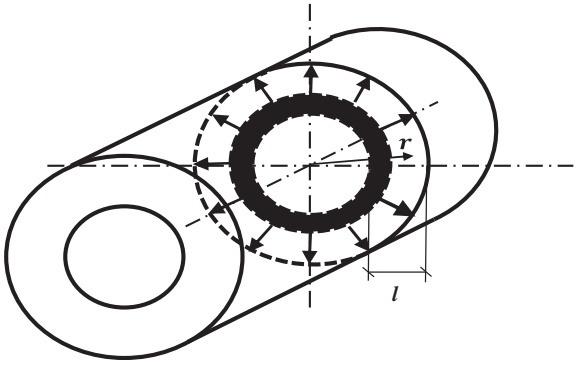

Fig. 15. Fully-circumferential crack propagating radially.

1. crack propagation along the circumference of the pipe (as shown in Fig. 14), that generates a fully-circumferential crack. This phenomenon can be modeled referring to the crack length (x_2), whose threshold value $X_{cr,2}$ is equal to $2\pi r_i = 754$ mm.
2. radial propagation of the fully-circumferential crack (as shown in Fig. 15); this phenomenon can be modeled referring to the crack depth (x_1), whose threshold $X_{cr,1}$ value is equal to $l = 9$ mm.

To obtain the crack growth rate dx_i/dN, the same procedure explained in Section 3.2.2 is followed and Eqs. (18)–(21) are used. Concerning the propagation of the circumferential crack, σ_z of Eq. (14) is related to the thermal fatigue loading to the fully-circumferential crack (Radu et al., 2007b). The stresses intensity factors $(K_I^i(\sigma_z, x_i))$ $i = 1, 2$ are computed by applying the BS 7910 procedure for a circumferential crack propagating along the circumference and the API 579 procedure for a fully-circumferential crack propagating radially (FITNET FFS – MK 7).

We suppose that:

- in the first stage of crack propagation, the crack depth $(x_1 = x_1^{in})$ is constant and we approximates the hollow cylinder to a flat plate (see Section 3.2.2 hypothesis for the evaluation of K_I)
- the propagation phenomenon is studied at the inner surface of the pipes ($\varphi = 0$, see Fig. 10).

Theoretical details are given in Appendix B. Tables 1 and 2 list the parameters $\bar{\delta} = (f, \theta_0, E, \alpha, v, k, n, C)$ and the distributions used to evaluate $\Delta K_{eff}^i(\sigma_z, x_i)$ and N (Chapuliot et al., 2005). The number of cycles (N) needed to propagate a fully-circumferential crack, starting from a circumferential crack onset, is given by:

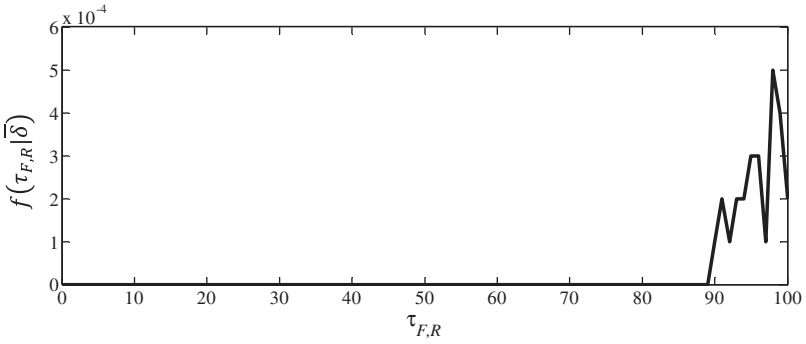

Fig. 16. Probability density function of the state holding time $\tau_{F,R}$.

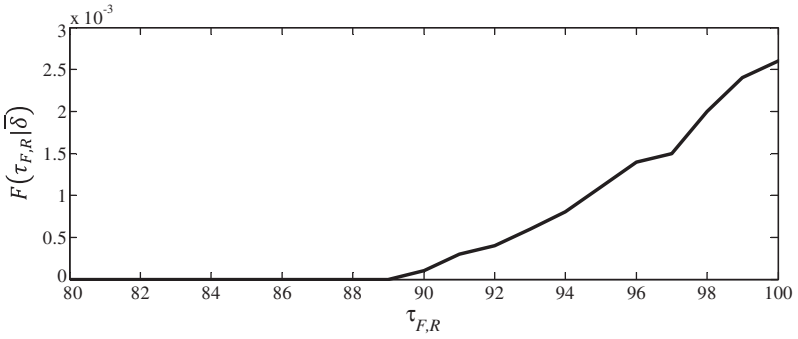

Fig. 17. Cumulative distribution function of the state holding time $\tau_{F,R}$.

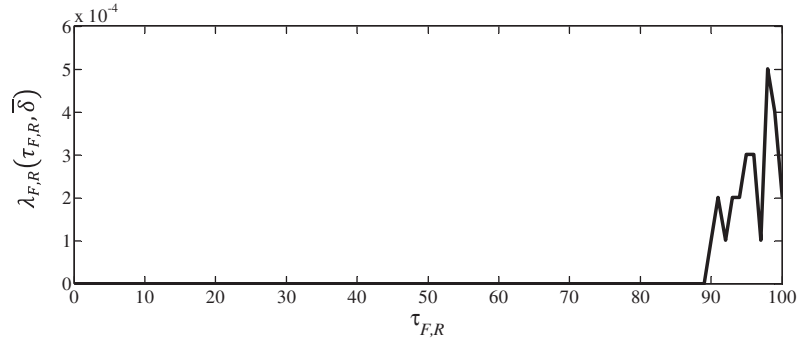

Fig. 18. Transition rate from state *F* to state *R*.

$$N = \int_{x_1^{in}}^{X_{cr,1}} \frac{dx_1}{C\cdot(\Delta K_{eff}^1(\sigma_z,x_1))^n} + \int_{x_2^{in}}^{X_{cr,2}} \frac{dx_2}{C\cdot(\Delta K_{eff}^2(\sigma_z,x_2))^n} \quad (24)$$

The equation has been solved using a MATLAB solver. The state holding time $\tau_{F,R}$ for a specific set of $\bar{\delta}$ affecting the radial propagation of the crack is, thus, calculated from *N* as:

$$\tau_{F,R}(years) = \frac{N}{f\cdot 3600\cdot 24\cdot 365} \quad (25)$$

The probability distribution of $\tau_{F,R}$ is estimated by applying the MC simulation proposed at item (4) of Section 2.2.1, with a number of trials $N_c = 10,000$. For each one of these N_c trials, $\Delta K_{eff}^i(\sigma_z,x_i)$ are evaluated given a sampled batch of values of the parameters $\bar{\delta}$ (Tables 1 and 2). Then, the distributions $f(\tau_{F,R}|\bar{\delta})$ and $F(\tau_{F,R}|\bar{\delta})$ can be built (shown in Figs. 16 and 17, respectively). By applying Eq. (6) with a time step of one year ($\Delta\tau = 1$), the transition rate $\lambda_{F,R}(\tau_{F,R},\bar{\delta})$ is computed (shown in Fig. 18).

The cumulative distribution function $F(\tau_{F,R}|\bar{\delta})$ describing the (uncertain) timing of one of the possible second steps of the degradation process (i.e., transition between states *F* and *R*), and shown in Fig. 17, shows that the transition between these two states can be considered very rare during the usual 40 years of a NPP life (once the component enter state *F* it has to wait at least $\tau_{F,R} = 89$ years to leave state *F* and enter state *R* with negligible $f(\tau_{F,R}|\bar{\delta})$ and $F(\tau_{F,R}|\bar{\delta})$). Again, the discontinuity and the irregularity of the curve representing the transition rate $\lambda_{F,R}(\tau_{F,R},\bar{\delta})$ can be explained as for the estimation of $\lambda_{F,L}(\tau_{F,L},\bar{\delta})$ of Section 3.2.2.

3.2.4. Transition rate $\lambda_{L,R}(\tau_{L,R})$

The transition between states Leak (*L*) (i.e., through-wall crack that presents leakage phenomena) and rupture (*R*) (i.e., the pipe

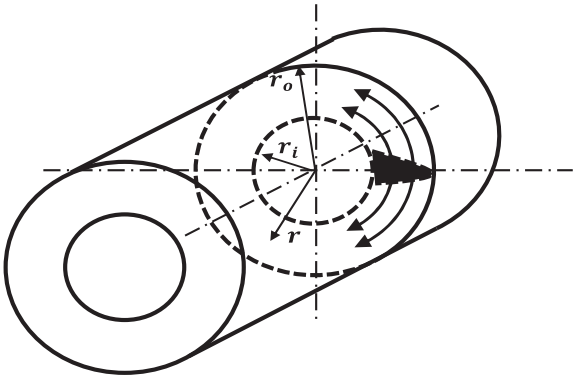

Fig. 19. Through-wall circumferential crack propagating along the circumference.

is completely broken), shown in Fig. 19, occurs when the crack length (x_2) has reached the circumference dimension in the outside surface of the pipe, that is equal to:

$$X_{cr,2} = 2\pi r_o = 819 \text{ mm} \tag{26}$$

Responsible for the crack propagation is the axial stress (σ_z), given in Eq. (14) (Radu et al., 2007b). To determine the number of thermal cycles N after which the system will experience a rupture, the same procedure explained in Section 3.2.2 is followed and Eqs. (18)–(21) are used. The stress intensity factor $(K_I(\sigma_z, x_2))$ is computed by applying the BS 7910 procedure for a through-wall circumferential crack propagating along the pipe circumference (FITNET FFS – MK 7). Theoretical details are given in Appendix B. Tables 1 and 2 list the parameters $\overline{\delta} = (f, \theta_0, E, \alpha, v, k, n, C)$ and their distributions used to evaluate $\Delta K_{eff}(\sigma_z, x_2)$ and N (Chapuliot et al., 2005). The number of cycles (N) needed to reach X_{cr}, starting from a through-wall crack, is given by:

$$N = \int_{x_2^{in}}^{X_{cr,2}} \frac{dx_2}{C \cdot (\Delta K_{eff}(\sigma_z, x_2))^n} \tag{27}$$

The initial crack length x_{in} is considered equal to $x_2^{in} = 28$ μm. The equation has been solved using a MATLAB solver. The state holding time $\tau_{L,R}$ for a specific set of $\overline{\delta}$ affecting the propagation of the crack is, then, calculated from N as:

$$\tau_{L,R} \text{ (years)} = \frac{N}{f \cdot 3600 \cdot 24 \cdot 365} \tag{28}$$

The probability distribution of $\tau_{L,R}$ is estimated by applying the MC simulation proposed at item (4) of Section 2.2.1, with a number of trials $N_c = 10,000$. For each one of these N_c trials, $\Delta K_{eff}(\sigma_z, x)$ is evaluated given a sampled batch of values of the parameters $\overline{\delta}$ (Tables 1 and 2). Then, the distributions $f(\tau_{L,R}|\overline{\delta})$ and $F(\tau_{L,R}|\overline{\delta})$ can be built (shown in Figs. 20 and 21, respectively). By applying Eq. (6) with a time step of one year $(\Delta\tau = 1)$, the transition rate $\lambda_{L,R}(\tau_{L,R}, \overline{\delta})$ is computed (shown in Fig. 22).

Figs. 20 and 22 show that once the crack reaches a circumferential through-wall characteristic, it rapidly propagates (peak value at the 3rd year). Moreover, the Figure shows that provided that the component is in state L, the transition out of this state into state R can occur with high probability.

3.2.5. Repair transition rates ω and μ

The repair rates ω and μ are estimated by means of two simple models described as follows (Fleming, 2004):

$\omega = \frac{P_I P_{FD}}{(T_{FI} + T_R)} = 2 \times 10^{-2}/\text{yr}$ components are assumed to have a 25% chance (P_I) of being inspected for flaws detection every 10 years (T_{FI}) with a 90% detection probability (P_{FD});

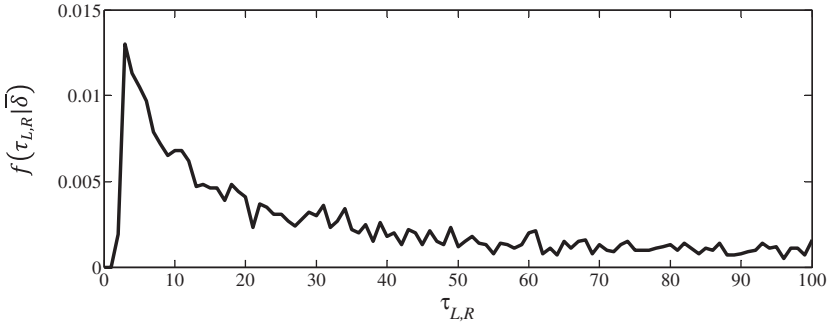

Fig. 20. Probability density function of the state holding time $\tau_{L,R}$.

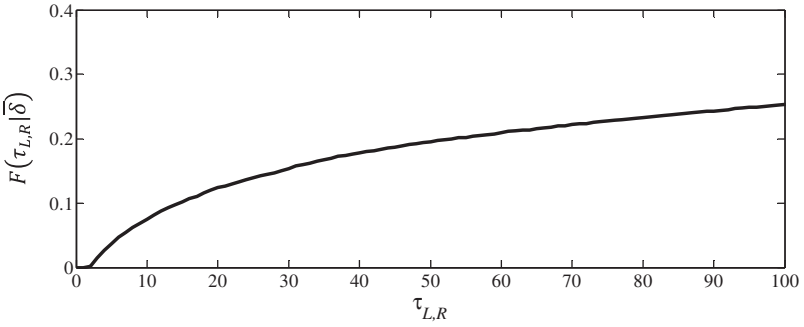

Fig. 21. Cumulative distribution function of the state holding time $\tau_{L,R}$.

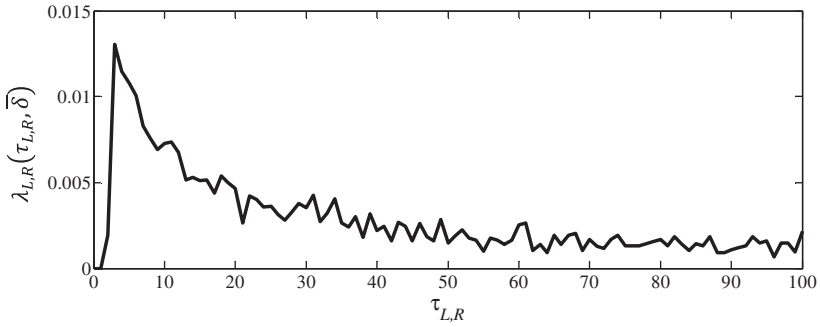

Fig. 22. Transition rate from states *L* to state *R*.

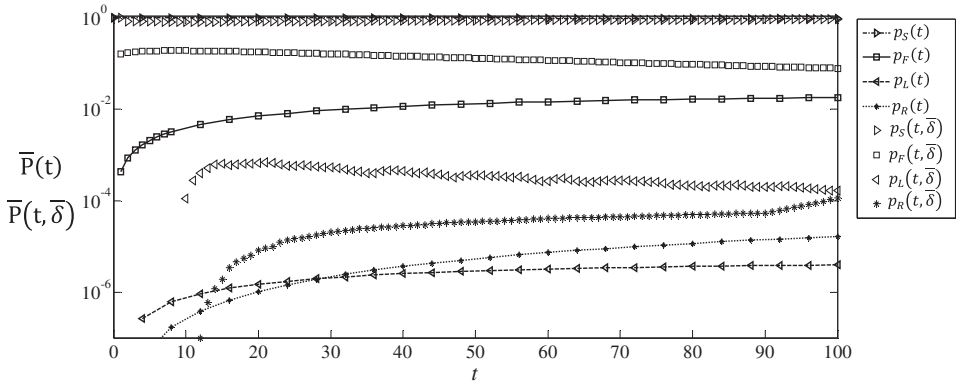

Fig. 23. State probability vector solution. Comparison of MCM and MSPM approaches.

$\mu = \frac{P_I P_{LD}}{(T_{LI}+T_R)} = 7.92 \times 10^{-1}$/yr

detected Flaws will be repaired in 200 h (T_R = 200 h/8760 h/year).
the components are assumed to have a 90% chance (P_I) of being inspected for leak detection every 1 years (T_{LI}) with a 90% detection probability (P_{LD});
detected Leaks will be repaired in 200 h (T_R = 200 h/8760 h/year).

These two transition rates are considered constant and the state transition time will follow an exponential distribution.

3.3. State probability $\overline{P}(t)$

To evaluate the probability vector solution $\overline{P}(t)$, the procedure explained in Section 2.2.2 is followed. Fig. 23 shows the solution of $\overline{P}(t,\overline{\delta})$ obtained with a MSPM whose transition rates values have been defined in the previous Sections and the solution obtained by solving an MCM as in Fleming (2004), in which the transition rates are considered constant so that the state holding times are exponentially distributed. Fig. 23 shows that the probabilities $p_L(t,\overline{\delta})$ and $p_R(t,\overline{\delta})$, obtained with the MSPM, are larger than $p_L(t)$ and $p_R(t)$ obtained by MCM (Fleming, 2004) due to $\lambda_{F,L}(\tau_{F,L},\overline{\delta})$ and $\lambda_{L,R}(\tau_{L,R},\overline{\delta})$ of Figs. 13 and 22. Moreover, it is worth noticing the decreasing trends of the $p_F(t,\overline{\delta})$ and $p_L(t,\overline{\delta})$: those phenomena can be explained looking at the distributions of the transition rates $\lambda_{F,L}(\tau_{F,L},\overline{\delta})$ and $\lambda_{L,R}(\tau_{L,R},\overline{\delta})$, shown in Figs. 13 and 22, that have decreasing trends as $p_F(t,\overline{\delta})$ and $p_L(t,\overline{\delta})$. This means that once the system enters states *F* or *L*, it has a larger probability to leave these states and enter states *L* or *R*, respectively, after a short time. With respect to the transition from state *F* to *R*, it can be seen that the distribution of $\lambda_{F,R}(\tau_{F,R},\overline{\delta})$ of Fig. 18 influences the $p_R(t,\overline{\delta})$ to be in state *R* at the very end of its life (90–100 years).

Indeed, the estimates provided by MCM (dotted line with diamonds) and MSPM (stars) differ from the early stage of the piping system operation. This is due to the fact that the integration in the MSPM of more physical information (data and models) than in MCM has allowed a more realistic degradation process modeling. As a result, below 15 years the probability of rupture is not credible for MCM (e.g., leading to a relaxation of maintenance/repair efforts, with cost savings when relying on the MSPM results), whereas at larger times the probability of rupture is underestimated by MCM (~1 order of magnitude), with the risk associated to this.

4. Conclusions

A Multi-State Physics Modeling (MSPM) framework for degradation modeling and failure probability quantification of Nuclear Power Plants piping systems has been developed.

The approach has been applied to a benchmark problem of a piping system of a Pressurized Water Reactor undergoing thermal fatigue. The results are compared with a continuous-time homogeneous Markov Chain Model (MCM).

The transition rates describing the degradation phenomenon in the MSPM have been determined by simulating the degradation (physics) models that describe the different stages of the thermal fatigue degradation process of a piping component and evaluating by Monte Carlo (MC) simulation the time-dependent transition rates between the states of the MSPM.

The comparison of the MCM with the MSPM results shows that with more realistic assumptions and consistent exploitation of the available knowledge (data and models), the latter method gives larger probabilities of occurrence of a leakage/rupture in the piping system, than the MCM. This difference in the estimates can be significant from the risk point of view, as this could be underestimated with all associated consequences. This shows the importance of finding "modeling ways" to include all the knowledge and information available (in the form of data, models, expert judgments, etc.) for an informed-as-possible, faithful-as-possible description of the real degradation and failure mechanism. Finally, another advantage of the MSPM for piping systems failure probability quantification is its applicability to assess the reliability of newly designed NPPs components when lacking of field data.

Appendix A. Thermal fatigue stresses solution

Thermal stresses due to thermal fatigue are dependent on the temperature distribution $\theta(r,\omega,\theta_0,k,t)$ across the wall thickness. For the simple geometry of a pipe that can be represented as a hollow cylinder, analytical solutions for temperature fields and associated elastic thermal stresses σ_r, σ_z, and σ_ϑ distributions for a pipe subject to sinusoidal transient thermal loading, have been developed in Radu et al. (2007a).

The one-dimensional heat diffusion equation in cylindrical coordinates and with axisymmetric thermal variations is (Radu et al., 2007a):

$$\begin{cases} \frac{\partial^2\theta}{\partial r^2}+\frac{1}{r}\frac{\partial\theta}{\partial r}=\frac{1}{k}\frac{\partial\theta}{\partial t} \\ \theta(r_i,t)=\theta_0\cdot\sin(\omega t) \\ \theta(r_0,t)=0 \\ \theta(r,0)=0 \end{cases} \tag{29}$$

where $\theta=T(r,t)-T_0$ and T_0, is the unstrained temperature.

The solution for the temperature distribution during a thermal transient can be written as follows (Radu et al., 2007a):

$$\theta(r,\omega,\theta_0,k,t)=k\cdot\pi\cdot\sum_{n=1}^{\infty}\theta_1(r_i,r_o,s_n)\cdot\theta_2(r_i,r,s_n)\cdot\theta_3(\omega,t,s_n) \tag{30}$$

where

$$\theta_1(r_i,r_o,s_n)=\frac{s_n^2\cdot J_0^2(s_n r_o)}{J_0^2(s_n r_o)-J_0^2(s_n r_i)} \tag{31}$$

$$\theta_2(r_i,r,s_n)=Y_0(s_n r_i)\cdot J_0(s_n r)-J_0(s_n r_i)\cdot Y_0(s_n r) \tag{32}$$

$$\theta_3(\omega,t,s_n)=\theta_0\cdot\frac{\omega\cdot e^{-k\cdot s_n^2\cdot t}+(k\cdot s_n^2)\cdot\sin(\omega t)-\omega\cdot\cos(\omega t)}{(k\cdot s_n^2)^2+\omega^2} \tag{33}$$

and s_n are the positive roots of

$$Y_0(s_n\cdot r_i)\cdot J_0(s_n\cdot r_o)-J_0(s_n\cdot r_i)\cdot Y_0(s_n\cdot r_o)=0 \tag{34}$$

where $J_v(z)$, $Y_v(z)$ are the Bessel functions of first and second kind of order (v).

The temperature distribution $\theta(r,\omega,\theta_0,k,t)$ has been used to calculate the thermal stress components. The one-dimensional equilibrium equation in the radial direction is (Radu et al., 2007a):

$$\frac{d\sigma_r}{dr}+\frac{\sigma_r-\sigma_\vartheta}{r}=0 \tag{35}$$

The displacement technique has been used to solve the axisymmetric problems of hollow cylinders. When all the strains and stresses are only functions of the radial distance r, the strain displacement relations are (Radu et al., 2007a):

$$\varepsilon_r=\frac{du}{dr}\quad \varepsilon_\vartheta=\frac{u}{r}\quad \varepsilon_{r\vartheta}=0 \tag{36}$$

where u is the radial displacement.

The components of stress in cylindrical coordinates can be expressed as (Radu et al., 2007a):

$$\sigma_r=\frac{E'}{1-\nu'^2}\left[\frac{du}{dr}+\nu'\cdot\frac{u}{r}-(1+\nu')\cdot\alpha'\cdot\theta+(1+\nu')\cdot c'\right] \tag{37}$$

$$\sigma_\vartheta=\frac{E'}{1-\nu'^2}\left[\nu'\cdot\frac{du}{dr}+\frac{u}{r}-(1+\nu')\cdot\alpha'\cdot\theta+(1+\nu')\cdot c'\right] \tag{38}$$

$$\sigma_{r\vartheta}=0 \tag{39}$$

substituting Eqs. (37) and (38) into Eq. (35), we get:

$$\frac{d}{dr}\left[\frac{1}{r}\cdot\frac{d(r\cdot u)}{dr}\right]=(1+\nu')\cdot\alpha'\cdot\frac{d\theta(r,t)}{dr} \tag{40}$$

and the general solution of Eq. (41) is:

$$u=(1+\nu')\cdot\alpha'\cdot\frac{1}{r}\cdot\int_r\theta(r,t)\cdot r\cdot dr+C_1\cdot r+\frac{C_2}{r} \tag{41}$$

where the constants E', ν', α', c' in Eqs. (37)–(39) are:

$$E'=\frac{E}{1-\nu^2}\quad \upsilon'=\frac{\upsilon}{1-\upsilon}\quad \alpha'=(1+\upsilon)\cdot\alpha\quad c'=\nu\cdot\varepsilon_0 \tag{42}$$

The radial, hoop and axial stresses for an hollow cylinder made of an homogeneous isotropic material are (Radu et al., 2007a):

$$\sigma_r(r,\omega,\theta_0,k,t)=\frac{\alpha\cdot E}{1-\nu}\cdot\left[-\frac{1}{r^2}\cdot I_1(r,\omega,\theta_0,k,t)+\frac{r^2-r_i^2}{r^2\cdot(r_o^2-r_i^2)}\cdot I_2(r,\omega,\theta_0,k,t)\right] \tag{43}$$

$$\sigma_\vartheta(r,\omega,\theta_0,k,t)=\frac{\alpha\cdot E}{1-\nu}\cdot\left[\frac{1}{r^2}\cdot I_1(r,\omega,\theta_0,k,t)+\frac{r^2-r_i^2}{r^2\cdot(r_o^2-r_i^2)}\cdot I_2(r,\omega,\theta_0,k,t)-\theta(r,\omega,\theta_0,k,t)\right] \tag{44}$$

$$\sigma_z(r,\omega,\theta_0,k,t)=\frac{\alpha\cdot E}{1-\nu}\cdot\left(\frac{2\nu}{r_o^2-r_i^2}\cdot I_2(r,\omega,\theta_0,k,t)-\theta(r,\omega,\theta_0,k,t)\right) \tag{45}$$

where $I_1(r,\omega,\theta_0,k,t)$ and $I_2(r,\omega,\theta_0,k,t)$ are expressed as:

$$\begin{aligned} I_1(r,\omega,\theta_0,k,t)&=\int_{r_i}^{r}\theta(r,\omega,\theta_0,k,t)\cdot r\cdot dr \\ &=k\cdot\pi\cdot\sum_{n=1}^{\infty}\frac{s_n^2\cdot J_0^2(s_n\cdot r_o)}{J_0^2(s_n\cdot r_o)-J_0^2(s_n\cdot r_i)} \\ &\times\left[\frac{1}{s_n}\{Y_0(s_n\cdot r_i)\cdot[r\cdot J_1(s_n\cdot r)-r_i\cdot J_1(s_n\cdot r_i)] \right. \\ &\left.-J_0(s_n\cdot r_i)\cdot[r\cdot Y_1(s_n\cdot r)-r_i\cdot Y_1(s_n\cdot r_i)]\}\right] \\ &\times\left[\theta_0\cdot\frac{\omega\cdot e^{-ks_n^2\cdot t}+(k\cdot s_n^2)\cdot\sin(\omega\cdot t)-\omega\cdot\cos(\omega\cdot t)}{(k\cdot s_n^2)^2+\omega^2}\right] \end{aligned} \tag{46}$$

$$I_2(r,\omega,\theta_0,k,t)=\int_{r_i}^{r_o}\theta(r,\omega,t)\cdot r\cdot dr = k\cdot\pi\cdot\sum_{n=1}^{\infty}\frac{s_n^2\cdot J_0^2(s_n\cdot r_o)}{J_0^2(s_n\cdot r_o)-J_0^2(s_n\cdot r_i)} \times\left[\frac{1}{s_n}\{Y_0(s_n\cdot r_i)\cdot[r_o\cdot J_1(s_n\cdot r)-r_i\cdot J_1(s_n\cdot r_i)] -J_0(s_n\cdot r_i)\cdot[r_o\cdot Y_1(s_n\cdot r_o)-r_i\cdot Y_1(s_n\cdot r_i)]\}\right] \times\left[\theta_0\cdot\frac{\omega\cdot e^{-ks_n^2\cdot t}+(k\cdot s_n^2)\cdot\sin(\omega\cdot t)-\omega\cdot\cos(\omega\cdot t)}{(k\cdot s_n^2)^2+\omega^2}\right] \quad (47)$$

For clarity sake, in Eqs. (12)–(14) t has not been reported.

Appendix B. BS 7910 procedure for flat plate $K_I(\sigma_m,\sigma_b,x_1,x_2)$ solution

In the BS 7910 procedure, the stress intensity factor $K_I(\sigma_m,\sigma_b,x_1,x_2)$ is expressed as a function of the stress intensity magnification factor for membrane (M_m) and bending (M_b) stresses, the finite width factor (f_w) and the linearized membrane $(\sigma_m(x_1))$ and bending $(\sigma_b(x_1))$ stresses over the position of the crack depth as (FITNET FFS – MK 7):

$$K_I(\sigma_m,\sigma_b,x_1,x_2)=f_w(x_1,x_2,l,w)\cdot[M_m(x_1,x_2,l)\cdot\sigma_m+M_b(x_1,x_2,l)\cdot\sigma_b]\sqrt{\pi x_1} \quad (48)$$

$M_m(x_1,x_2,l)$ and $M_b(x_1,x_2,l)$, functions of the crack depth (x_1) and crack length (x_2) and of the wall thin (l), are equal to (FITNET FFS – MK 7):

$$M_m=\left[M_1+M_2\cdot\left(\frac{x_1}{l}\right)^2+M_3\cdot\left(\frac{x_1}{l}\right)^4\right]\frac{gf_\vartheta}{\Phi} \quad (49)$$

$$M_b=M_m[H_1+(H_2-H_1)(\sin\varphi)^q] \quad (50)$$

where M_1, M_2, M_3, Φ, H_1, H_2, q, are given in the following Eqs. (51)–(57) and Eqs. (58)–(64) for a ratio of $x_1/x_2\leqslant 0.5$ and $0.5<x_1/x_2\leqslant 1$, respectively (FITNET FFS – MK 7).

$$M_1=1.13-0.09\cdot\left(\frac{x_1}{x_2/2}\right) \quad (51)$$

$$M_2=\left[\frac{0.89}{0.2+\left(\frac{x_1}{x_2/2}\right)}\right]-0.54 \quad (52)$$

$$M_3=0.5-\frac{1}{0.65+\frac{x_1}{x_2/2}}+14\left(1-\frac{x_1}{x_2/2}\right)^{24} \quad (53)$$

$$\Phi=\sqrt{1-1.464\cdot\left(\frac{x_1}{x_2/2}\right)^{1.65}} \quad (54)$$

$$H_1=1-0.34\cdot\left(\frac{x_1}{l}\right)-0.11\cdot\left(\frac{x_1}{l}\right)\cdot\left(\frac{x_1}{x_2/2}\right) \quad (55)$$

$$H_2=1-\left[-1,22+0.12\cdot\left(\frac{x_1}{x_2/2}\right)\right]\cdot\left(\frac{x_1}{l}\right)-\left[0.55-1.05\cdot\left(\frac{x_1}{x_2/2}\right)^{0.75}+0.47\cdot\left(\frac{x_1}{x_2/2}\right)^{1.5}\right]\cdot\left(\frac{x_1}{l}\right)^2 \quad (56)$$

$$q=0.2+\left(\frac{x_1}{x_2/2}\right)+0.6\cdot\left(\frac{x_1}{l}\right) \quad (57)$$

$$M_1=\left(\frac{x_2/2}{x_1}\right)^{0.5}\left[1-0.04\cdot\left(\frac{x_2/2}{x_1}\right)\right] \quad (58)$$

$$M_2=0.2\cdot\left(\frac{x_2/2}{x_1}\right)^4 \quad (59)$$

$$M_3=-0.11\cdot\left(\frac{x_2/2}{x_1}\right)^4 \quad (60)$$

$$\Phi=\sqrt{1-1.464\cdot\left(\frac{x_2/2}{x_1}\right)^{1.65}} \quad (61)$$

$$H_1=1-\left[0.04+0.41\cdot\left(\frac{x_2/2}{x_1}\right)\right]\cdot\left(\frac{x_1}{l}\right)+\left[0.55-1.93\cdot\left(\frac{x_2/2}{x_1}\right)^{0.75}+1.38\cdot\left(\frac{x_2/2}{x_1}\right)^{1.5}\right]\cdot\left(\frac{x_1}{l}\right)^2 \quad (62)$$

$$H_2=1-\left[-2.11+0.77\cdot\left(\frac{x_2/2}{x_1}\right)\right]\cdot\left(\frac{x_1}{l}\right)-\left[0.55-0.72\cdot\left(\frac{x_2/2}{x_1}\right)^{0.75}+0.14\cdot\left(\frac{x_2/2}{x_1}\right)^{1.5}\right]\cdot\left(\frac{x_1}{l}\right)^2 \quad (63)$$

$$q=0.2+\left(\frac{x_2/2}{x_1}\right)+0.6\cdot\left(\frac{x_1}{l}\right) \quad (64)$$

For the parameters g and f_ϑ, we used the simplified values listed in Table 3 (FITNET FFS – MK 7).

The finite width factor (f_w) is expressed as Eq. (65), where the surface width $W=2\pi r_m$ and r_m is the mean radius of the pipe (FITNET FFS – MK 7):

$$f_w=\left[sec\left[\left(\frac{\pi x_2/2}{W}\right)\sqrt{\left(\frac{x_1}{l}\right)}\right]\right]^{0.5} \quad (65)$$

The linearized stresses $\sigma_m(x_1)$ and $\sigma_b(x_1)$ (MPa), functions of the crack depth, take values from the analytical stresses distributions computed as in Appendix A. $\sigma_m(x_1)$ and $\sigma_b(x_1)$ are expressed as (FITNET FFS – MK 7):

$$\sigma_m(x_1)=\frac{4Nx_1^2-6Mx_1-3Nlx_1+6Ml}{x_1^3} \quad (66)$$

Table 3
Simplified values for g and f_ϑ parameters.

	$\varphi=\pi/2$		$\varphi=0$	
	$x_1/x_2\leqslant 0.5$	$0.5<x_1/x_2\leqslant 1$	$x_1/x_2\leqslant 0.5$	$0.5<x_1/x_2\leqslant 1$
g	1	1	$1.1+0.35\cdot(x_1/l)^2$	$1.1+0.35\cdot\left(\frac{x_2/2}{x_1}\right)\cdot(x_1/l)^2$
f_ϑ	1	$\left(\frac{x_2/2}{x_1}\right)^{0.5}$	$(x_1/c)^{0.5}$	1

$$\sigma_b(x_1) = \frac{3Nlx_1 - 6Ml}{x_1^3} \tag{67}$$

where the parameters N and M are:

$$N = \int_0^{x_1} \sigma(r_n) dr_n \tag{68}$$

$$M = \int_0^{x_1} x\sigma(r_n) dr_n \tag{69}$$

In this work, $\sigma(r_n)$ is the 4th order polynomial expression fitted to the through-wall stress profile σ_z in the radial direction (that corresponds to the crack propagation direction) of the hollow cylinder, for an instant of time t_i^s into the sinusoidal period, and r_n is the radial coordinate starting at the inner surface of the pipe.

To evaluate the stress intensity factor, the following steps must be followed:

1. Evaluate i 4th order polynomial expressions, fitted to the stress profiles in radial direction of σ_z, given in Eqs. (13) and (14), for different times t_i^s $i = 1, 2, \ldots, n$ in the entire sinusoidal period, as a function of the normalized radial distance $\frac{r_n}{l}$, for t_i^s $i = 1, 2, \ldots, n$ (Radu et al., 2007b):

$$\sigma_i(r_n/l) = \sigma_0 + \sigma_1 \cdot \left(\frac{r_n}{l}\right) + \sigma_2 \cdot \left(\frac{r_n}{l}\right)^2 + \sigma_3 \cdot \left(\frac{r_n}{l}\right)^3 + \sigma_4 \cdot \left(\frac{r_n}{l}\right)^4 \tag{70}$$

2. Evaluate $\sigma_m(x_1)$ and $\sigma_b(x_1)$ for n steps of crack dimension, until it reaches a selected threshold value (X_{cr}), for each of the i $\sigma_i(r_n/l)$.
3. Evaluate $K_I(\sigma_m, \sigma_b, x_1, x_2)$ applying Eq. (49).
4. For each crack growth step n, select the maximum and minimum values the $K_I(\sigma_m, \sigma_b, x_1, x_2)$ among the entire sinusoidal period.
5. Evaluate ΔK_{eff} , function of crack depth x_1 as explained in Section 3.2.2, by fitting with a cubic spline interpolation (e.g. using the MATLAB function) to use in the Paris law equation.

B.1. API 579 procedure for a fully circumferential crack $K_I(\sigma(r_n/l), x_1)$ solution

$K_I(x_1)$ is evaluated following API 579 procedure, as (Radu et al., 2007b):

$$K_I\left(\frac{x_1}{l}\right) = \left[G_0 \cdot \sigma_0 + G_1 \cdot \sigma_1 \cdot \left(\frac{x_1}{l}\right) + G_2 \cdot \sigma_2 \cdot \left(\frac{x_1}{l}\right)^2 + G_3 \cdot \sigma_3 \cdot \left(\frac{x_1}{l}\right)^3 + G_4 \cdot \sigma_4 \cdot \left(\frac{x_1}{l}\right)^4\right] \cdot \sqrt{\frac{\pi x_1}{Q}} \tag{71}$$

where σ_j, $j = 0, 1, 2, 3, 4$, are the coefficients of the polynomial stress distribution (MPa), $Q = 1$ and the coefficients G_0, G_1, G_2, G_3, G_4, are expressed in Eqs. (76)–(80), respectively, (Radu et al., 2007b) for a fully-circumferential crack, and a ratio $r_i/l = 13$.

$$G_0\left(\frac{x_1}{l}\right) = 1.1198 + 0.1938 \cdot \left(\frac{x_1}{l}\right) + 2.9663 \cdot \left(\frac{x_1}{l}\right)^2 - 0.5521 \cdot \left(\frac{x_1}{l}\right)^3 \tag{72}$$

$$G_1\left(\frac{x_1}{l}\right) = 0.6812 + 0.1654 \cdot \left(\frac{x_1}{l}\right) + 0.7604 \cdot \left(\frac{x_1}{l}\right)^2 + 0.1385 \cdot \left(\frac{x_1}{l}\right)^3 \tag{73}$$

$$G_2\left(\frac{x_1}{l}\right) = 0.5234 + 0.1608 \cdot \left(\frac{x_1}{l}\right) + 0.1388 \cdot \left(\frac{x_1}{l}\right)^2 + 0.3354 \cdot \left(\frac{x_1}{l}\right)^3 \tag{74}$$

Table 4
M_m function of λ_M for l/r_m =0.0723.

λ_M	M_m	M_b
0	1	1
1	1.214	0.624
2	1.612	0.404
3	2.020	0.319
4	1.382	0.278
5	1.711	0.265
6	2.214	0.490
7	1.509	0.352
8	1.844	0.295
9	2.467	0.273

$$G_3\left(\frac{x_1}{l}\right) = 0.4391 + 0.1557 \cdot \left(\frac{x_1}{l}\right) - 0.1345 \cdot \left(\frac{x_1}{l}\right)^2 + 0.4271 \cdot \left(\frac{x_1}{l}\right)^3 \tag{75}$$

$$G_4\left(\frac{x_1}{l}\right) = 0.3785 + 0.0937 \cdot \left(\frac{x_1}{l}\right) + 0.0151 \cdot \left(\frac{x_1}{l}\right)^2 + 0.2211 \cdot \left(\frac{x_1}{l}\right)^3 \tag{76}$$

Following the points 1.–4. in Appendix B Section 1, the stress intensity factor, function of crack depth, is evaluated.

B.2. BS 7910 procedure for a through-wall circumferential crack $K_I(\sigma(r_n/l), x_2)$ solution

The stress intensity factor is evaluated considering the following hypothesis:

1. The crack length is evaluated on the outside surface of the pipe.
2. Membrane (σ_m) and bending (σ_b) stresses are obtained applying Eqs. (66)–(69) with $x_1 = 9$ mm.

The stress intensity factor $(K_I(x_2))$ can be expressed as (FITNET FFS – MK 7):

$$K_I(x_2) = (M_m\sigma_m + M_b\sigma_b)\sqrt{\pi x_2} \tag{77}$$

where M_m and M_b are expressed as in Table 4 as a function of λ_M that is equal to (FITNET FFS – MK 7):

$$\lambda_M = \left[12 \cdot (1 - \nu^2)\right]^{0.25} \frac{x_2/2}{\sqrt{r_m}} \tag{78}$$

Following the points 1.–4. in Appendix B Section 1, the stress intensity factor, function of crack depth, is evaluated.

References

Ancelet, O., Chapuliot, S., Henaff, G., Marie, S., 2007. Development of a test for the analysis of the harmfulness of a 3D thermal fatigue loading in tubes. Int. J. Fatigue 29, 549–564.

Bush, S.H., Do, M.J., Slavich, A.L., Chockie, A.D., 1996. Piping failures in the US nuclear power plants 1961–1995. prepared by Chockie Group International Inc., for Swedish Nuclear Power Inspectorate, SKI Report 96:20.

Chapuliot, S., Gourdin, C., Payen, T., Magnaud, J.P., Monavon, A., 2005. Hydro-thermal-mechanical analysis of thermal fatigue in a mixing tee. Nucl. Eng. Des. 235, 575–596.

Chatterjee, K., Modarres, M., 2008. A Probabilistic Physics of Failure Approach to Prediction of Steam Generator Tube Rupture Frequency. ANS PSA 2011 International Topical Meeting on Probabilistic Safety Assessment and Analysis Wilmington, NC, March 13–17, 2011, on CD-ROM. American Nuclear Society, LaGrange Park.

Di Maio, F., Zio, E., 2013. Failure prognostics by a data-driven similarity-based approach. Int. J. Reliab. Qual. Saf. Eng. 20(2) (1), 1–17.

FITNET Fitness-for-Service PROCEDURE, 2006. Prepared by European Fitness-for-Service Thematic Network – FITNET.

Fleming, K.N., 2004. Markov models for evaluating risk-informed in-service inspection strategies for nuclear power plant piping systems. Reliab. Eng. Syst. Saf. 83, 27–45.

Fleming, K.N., Smit, K., 2008. Evaluation of design, leak monitoring, and NDE strategies to assure PBMR helium pressure boundary reliability, In: Proceeding of the Fourth International Topical Meeting on High Temperature Reactor Technology, HTR 2008, September 28, October 1, Washington, DC, USA.

Gopika, V., Bidhar, S.K., Kushwaha, H.S., Verma, A.K., Srividya, A., 2003. A comprehensive framework for evaluation of piping reliability due to erosion–corrosion for risk-informed inservice inspection. Reliab. Eng. Syst. Saf. 82, 187–193.

Gosselin, S.R., Fleming, K.N., 1997. Evaluation of pipe failure potential via degradation mechanism assessment. In: Proceedings of ICONE 5, Fifth International Conference on Nuclear Engineering, May 26–30, Nice, France.

Kozin, F., Bogdonoff, J.L., 1989. Probabilistic model of fatigue crack growth: results and speculation. Nucl. Eng. Des. 115, 143–171.

Li, Y.F., Zio, E., Lin, Y.H., 2012. A multi-state physics model of component degradation based on stochastic petri nets and simulation. IEEE Trans. Reliab. 61 (4), 921–931.

Lisnianski, A., Frenkel, I., Khvatskin, L., Ding, Y., 2008. Maintenance contract assessment for aging systems. Qual. Reliab. Eng. Int. 24, 519–531.

Radu, V., Paffumi, E., Taylor, N., 2007. New analytical stress formulae for arbitrary time dependent thermal loads in pipes, EUR 22802 EN.

Radu, V., Paffumi, E., Taylor, N., Nilsson, K.-F., 2007. Assessment of thermal fatigue crack growth in the high cycle domain under sinusoidal thermal loading, EUR 23223EN.

Sester, M., Chauvot, C., Westerheide, R., Heilmann, A., 2000. Analysis and assessment of the damage mechanisms in austenitic power plant components subjected to mechanical and thermocyclic loading, Report T 12/2000, Fraunhofer IWM, Freiburg and Halle.

Simola, K., Pulkkinen, U., Talja, H., Saarenheimo, S., Karjalainen-Roikonen, P., 2002. Comparative study of approaches to estimate pipe break frequencies. Nordic Nuclear Safety Research (NKS) SOS-2 Project Espoo.

Unwin, S.D., Lowry, P.P., Layton, R.F., Heasler, P.G., Toloczko, M.B., 2011. Multi-state physics models of aging passive components in probabilistic risk assessment. In: Proceedings of ANS PSA 2011 International Topical Meeting on Probabilistic Safety Assessment and Analysis, pp. 1–12.

Varfolomeyev, I., 2006. Computational modelling of crack initiation in a mixing tee subjected to thermal fatigue load. In: Proceedings of the 16th European Conference of Fracture, Alexandroupolis, Greece, July 3–7, pp. 213-214.

Verma, A.K., Srividya, A., Gopika, V., Rao, K.D., 2011. Risk-informed decision making in nuclear power plants. In: Hoang Pham, (Ed.), Safety and Risk Modeling and its Application, Springer Series in Reliability Engineering, London, http://dx.doi.org/10.1007/978-0-85729-470-8_12.

Zio, E., Di Maio, F., 2012. Fatigue crack growth estimation by relevance vector machine. Expert Syst. Appl. 39, 10681–10692.

Zio, E., Pedroni, N., 2011. How to effectively compute the reliability of a thermal-hydraulic nuclear passive system. Nucl. Eng. Des. 241, 310–327.